Polymer Testing 128 (2023) 108235

Contents lists available at ScienceDirect

Polymer Testing

journal homepage: www.elsevier.com/locate/polytest

Enhancement of the rheological properties of magnetorheological foam via different constraint volumes foaming approach

Ainaa Amirah Marzuki [a], Nur Azmah Nordin [a,*], Saiful Amri Mazlan [a], Mohd Aidy Faizal Johari [a], Rahayu Emilia Mohamed Khaidir [a], Michal Sedlacik [b,c,**], Ubaidillah [d]

[a] Engineering Materials and Structures (eMast) iKhoza, Malaysia – Japan International Institute of Technology (MJIIT), University Teknologi Malaysia, Jalan Sultan Yahya Petra, Kuala Lumpur, 54100, Malaysia
[b] Centre of Polymer Systems, University Institute, Tomas Bata University in Zlín, Trida T. Bati 5678, 760 01, Zlín, Czech Republic
[c] Department of Production Engineering, Faculty of Technology, Tomas Bata University in Zlín, Vavreckova 275, 760 01, Zlín, Czech Republic
[d] Mechanical Engineering Department, Faculty of Engineering, Universitas Sebelas Maret, Surakarta, 57126, Indonesia

ARTICLE INFO

Keywords:
Constrained foaming
Magnetorheological foam
Morphological properties
Rheological properties

ABSTRACT

The potential of magnetorheological (MR) foam, a recently developed porous smart material, has grown rapidly in recent years. The ability of MR foam to change its properties continuously, actively, and reversibly in response to a controlled external magnetic stimulus is one of its advantages for applications in advanced technology industries. However, its ability to store energy is still relatively low. This study attempts to address this drawback by highlighting a method to improve this ability by enhancing the material's storage modulus by introducing constrained foaming during the fabrication process. MR foam containing 75 wt% carbonyl iron particles (CIPs) was prepared in situ using two foaming approaches: free and constrained foaming. The effect of constraint foaming on the storage modulus enhancement was further investigated by reducing the mold length by 25 % and 50 %. The rheological properties of the fabricated MR foam samples were then examined using a rheometer in both the absence and presence of magnetic fields in an oscillatory shear mode. Thus, this study showed that constraint foaming has successfully improved the properties, especially regarding storage modulus and MR effect. When the mold volume was further reduced by 50 %, the storage modulus increased by about 50 % compared to a free-foaming MR foam at off-state conditions. Meanwhile, the results portrayed a higher storage modulus value under a 0.659 T magnetic field. This positive enhancement was believed to be due to a more compact CIP distribution. Hence, constraint volume MR foams were able to form stronger chain-like structures. The micrograph analysis by digital microscope revealed that the pore size decreased as the mold length was reduced. A shorter mold resulted in a more compact distribution of magnetic particles. As a result, MR foam with constrained foaming, especially at 50 % mold length, has a higher storage modulus. Overall, using constrained foaming to fabricate MR foam could improve the structure and mechanical properties of MR foam for a wide range of smart devices.

1. Introduction

The potential of magnetorheological (MR) foam as a smart material for high-technology and material science technology has been growing rapidly due to its ability to reversibly change its viscoelastic properties while quickly responding to an external magnetic field [1]. Categorized under solid-type MR materials, MR foam was at first developed to overcome sedimentation, leaking, and sealing issues accounted by liquid and semi-solid MR materials for specific applications, such as soft sensors and a few other types of sensor technology [2,3]. Magnetorheological foam has a porous structure, making it lightweight, flexible, and durable [4]. In general, the properties of a porous material are highly dependent on the pore structure [5]. Therefore, the fabrication process of MR foam plays an important role in producing a great quality MR foam. Previous studies have introduced a few approaches, mainly focused on producing porous materials with high porosity, low density, and high mechanical properties [6–9].

Within the last decades, much attention has been dedicated to

* Corresponding author.
** Corresponding author. Centre of Polymer Systems, University Institute, Tomas Bata University in Zlín, Trida T. Bati 5678, 760 01, Zlín, Czech Republic.
E-mail addresses: nurazmah.nordin@utm.my (N.A. Nordin), msedlacik@utb.cz (M. Sedlacik).

https://doi.org/10.1016/j.polymertesting.2023.108235
Received 12 July 2023; Received in revised form 14 September 2023; Accepted 4 October 2023
Available online 4 October 2023

developing and controlling the foam properties because the matrix material's and microstructure's behavior significantly impacts its performance [10]. It is noted that the pore distribution and size are key factors in facilitating the material's performance [11]. A few fabrication approaches have been proposed to produce porous structure materials, such as utilizing an injection molding, varying the flexibility of foam matrices, and using additives. Among these approaches, a constrained foaming process has been used as a reliable approach to regulating the structure of the pores [12,13]. The reproducibility of foam fabricated using this approach has significantly increased, up to 72 %, compared to the common free-foaming method [14]. A few factors contributed to this result, mainly the constrained foaming process limits the area for the foam to expand, thus reducing the pores collapse issue. In addition, the cell growth rate was significantly slower under the approach mentioned above, resulting in smaller pores, thus improving the impact strength of the foam [15]. Improvement of the foam properties, in terms of its compression and mechanical properties, was also put into spotlight. It was reported [16,17] that the constrained foaming approach effectively attracted more carbon dioxide to participate in the pores' nucleation and growth, producing lighter weight and higher foam strength. Over the years, the constrained foaming process has been further improved by introducing additives into the matrix materials. Nar et al. [18] studied the effect of adding a well-dispersed kenaf core fiber in the foam using a constrained approach, and their study contributed positively to the compressive and flexural properties of the composite foam. Furthermore, the presence of additives during the constrained foaming process improved the homogeneity of pores nucleation [19]. Therefore, this foam process would be considered a systematic approach to controlling the pore morphology, enhancing the resulting corresponding properties.

Even though there are few studies on the constrained foaming process of foam or composite foams, this approach has not been applied to fabricate the MR foam. Generally, few studies have been conducted on this smart material. Magnetorheological foam commonly comprises two main components: the polymer matrix and magnetic particles as fillers. Previous research has significantly discussed the polymer matrix as it influenced the properties of MR foam [20–23]. Thus, a compatible state of the polymer matrix, which possesses either rigid or flexible conditions, was considered to produce MR foam with desirable properties, such as enhanced storage modulus, $G^{'}$, and MR effect. The magnetic particles, usually CIPs, are eventually embedded into the struts of the foam porous structure during the forming process. Muhazeli et al. [21] studied the rigid MR foam and observed the effect of various magnetic particle concentrations on the properties of MR foam. Morphological analysis showed that MR foam embedded with 70 wt% of CIPs has smaller pores than foam without CIPs. Regarding the rheological results, the MR foam with smaller pores exhibited an increased MR effect of up to 35 %. However, a higher amount of CIPs caused the composite foam to be more brittle due to lower matrix material content. Meanwhile, in another study, Rizuan et al. [22] introduced an improved, flexible MR foam to overcome the brittleness issue while maintaining its performance. They revealed that 75 wt% was the best CIP concentration, which possessed the highest $G^{'}$ of up to 75 kPa.

Yet, the achievable $G^{'}$ of MR foam is still relatively low. According to Zaidi et al. [23], smart robotic applications such as soft grippers required higher $G^{'}$ up to 100 kPa for the application to work at the best performance. Hypothetically, the rheological properties of MR foam can be further improved by modifying the foam's physical properties. Thus, incorporating constrained foaming process during fabrication of MR foam is considered as an alternative effective approach to control the physical properties of MR foam, while it simultaneously improves the rheological properties. Thereupon, this study provides scientific evidence related to the effect of constrained foaming towards the enhancement of the composite porous materials and their characteristics. Different volumes of MR foam were produced by manipulating the height of mold used in accordance to the volume foaming approach. It is expected that by controlling the volume of MR foam, it able to regulate the structure of pores thereby improve the properties of MR foam.

2. Experimental method

2.1. Materials and sample preparation

MR foam consists of two main components: base matrix and magnetic particles. The matrix material used to fabricate the MR foam samples was flexible polyurethane (PU) in liquid form, supplied by Smooth On. Inc., USA. The PU foam was primarily a mixture of two parts, namely polyol and isocyanate. In particular, polyether polyol (PPG)-based triol was as a chemical agent with the density of 1.03 g/ml, whereas 4,4′-methylene bis (phenyl isocyanate) benzene was a chemical reactant that helped the formation of gas bubbles during the foaming process of the MR foam. The density of this chemical reactant was 1.00 g/ml. Meanwhile, to make it magnetically responsive, CIP was used as the magnetic particle because it has high saturation magnetization, permeability, and low remnant magnetization [24,25]. This OM grade CIP has spherical shapes with an average diameter ranging from 3 to 5 μm and was purchased from BASF, Ludwigshafen, Germany. The density of CIPs was approximately 7.87 g/ml.

The experimental procedure for the sample preparation was as follows. Firstly, MR foam was prepared with a fixed 75 wt% of CIPs via an in-situ polymerization method under an isotropic curing condition. The magnetic particles were mixed with polyol and stirred for 20 s using a mechanical stirrer at 550 rpm. Then, isocyanate was added to the mixture and stirred at the same stirring speed and duration. The final mixture was immediately poured into a 3-cm diameter cylindrical polyvinyl chloride mold for the foaming process to take place and was left curing at room temperature of 25 °C for 24 h. This study began with a no-restriction foaming procedure known as the open mold method. The foam height produced was observed and was later set as the maximum mold height for the closed mold method for the constrained foaming process.

Fig. 1 depicted an illustration of fabricated samples. The same free foaming fabrication method was conducted several times to ensure the heights obtained were dependable. Thus, the maximum height obtained during this process was set as 100 % length of the closed mold for the use of constrained foaming fabrication process. Lastly, the constrained foaming experiment was repeated with the length of the closed mold reduced by 25 % and 50 % from its original length. Table 1 tabulates the details on the fabricated MR foams.

2.2. Sample analysis and characterization

The fundamental parameters of porous materials were pores-related indicators, such as density (ρ) and porosity (φ) as it was reported to significantly influence the properties of the material [25–27]. Density measured on how much mass is concentrated within a given volume of a material, whereas porosity is described as the voids or empty spaces within a material. In this work, the density was calculated by the ratio of mass and geometric volume of the fabricated PU and MR foams. Then, the porosity was estimated by calculating the percentage of the inverse relative density $(\rho_{relative})$ [28–30] in which, the $\rho_{relative}$ has been defined by the ratio of the foam density (ρ_{sample}) and the solid density (ρ_{solid}) [31,32]. Equations (1)–(3) were used to calculate the ρ_{sample}, $\rho_{relative}$ and φ in this study respectively.

$$\rho_{sample}, g \Big/ ml = \frac{Mass\ of\ sample}{Volume\ of\ sample} \tag{1}$$

$$\rho_{relative} = \frac{\rho_{sample}}{\rho_{solid}} \tag{2}$$

$$Porosity\ (\varphi), \% = (1 - \rho_{relative}) \times 100\% \tag{3}$$

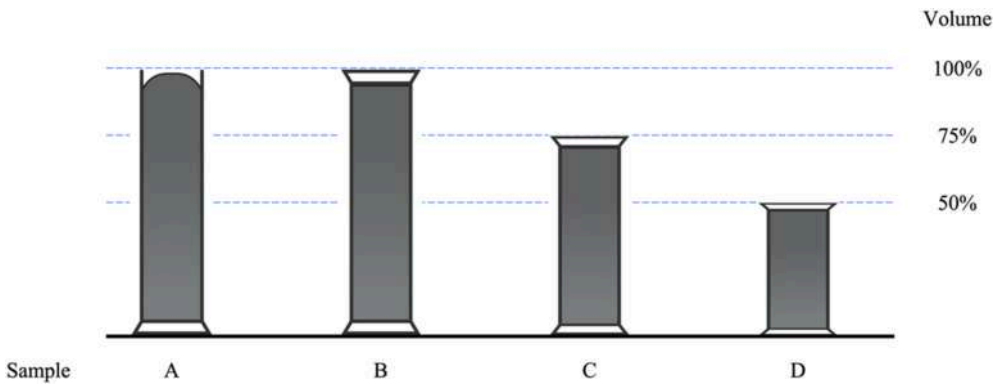

Fig. 1. Illustration of the fabricated MR foam, particularly sample A, B, C and D that representing free foaming, constraint foaming 100%, 75% and 50%, respectively.

Table 1
Foaming condition and volume of mold of fabricated MR foam.

Sample	Foaming condition	Volume of mold (%)
A	Free foaming	100
B	Constrained foaming	100
C	Constrained foaming	75
D	Constrained foaming	50

The rheological properties of the fabricated MR foams were analyzed using a modular compact rheometer (MCR302) from Anton Paar, Austria, equipped with a 20-mm diameter controllable parallel plate (PP20/MRD/T1P2). The gap between the parallel plates was set to 1 mm during the analysis. The MR foam was cut into samples of 1-mm thickness with 20-mm diameter. Since MR foam was a type of magnetic-conductive material, the rheological analysis was conducted in the absence and presence of a magnetic field. Generally, the magnetic field was generated at a right angle to the plane of the base plate and passed through the samples. A magnetic housing known as a yoke was employed to enclose the magnetic generator and ensured a consistent magnetic field was applied to the samples. Fig. 2 (a) and (b) depict a close-up image of the rheometer and its schematic diagram. The dotted lines in Fig. 2 (b) illustrate the magnetic field. Hence, it represents a conceptual representation of magnetic flow within the rheometer. Such an ideal operational scenario was typically supplied by the manufacturer. Correspondingly, note that simulating the actual field flow was not within the ambit of this study.

Subsequently, the rheological analysis was conducted as follows. The sample was placed through an oscillatory shear mode test to examine how the free and constrained foaming approach with varied mold volume affected the viscoelastic properties of the MR foam, particularly in terms of G' and MR effect. The properties of MR foam were analyzed by varying input parameters of 0.001–10 % sweep strains with a constant frequency of 1 Hz. In addition, different current magnitudes were applied to the samples to observe their behavior in the absence (0 A) and presence (1–4 A) of a magnetic field. It was noted that the current of 0, 1, 2, 3, and 4 A were equivalent to 0.003, 0.175, 0.356, 0.519, and 0.659 T, respectively. The test was conducted to evaluate the elasticity and deformation value of the MR foam by determining the linear viscoelastic (LVE) range.

On the other hand, the magnetic flux density, B, was manipulated during current sweep tests, commonly known as the magnetic field-dependent tests, to study the absolute MR effect of the fabricated MR foam. Particularly, the current was varied within the range of 0–5 A, which was approximately equivalent to the magnetic flux density of 0–0.774 T. The absolute MR effect was determined by calculating the difference between the initial and maximum values of G' that was obtained within the range of the applied magnetic field. All samples were tested at room temperature of 25 °C, and for each sample, a 30-point interval was set for every measurement for observation.

Nevertheless, the morphological analysis was done using an optical microscope (OM) to observe the pore structure of the fabricated MR foams. The analysis was conducted at room temperature of 25 °C, and the images were taken under ×50 magnification. Then, the number of nucleated pores was observed by calculating ratio between the number of pores per unit area of 1 mm^2 and its $\rho_{relative}$. Five areas were observed for each sample, and the average from the overall data obtained was taken as the final result. In addition, another morphological analysis was

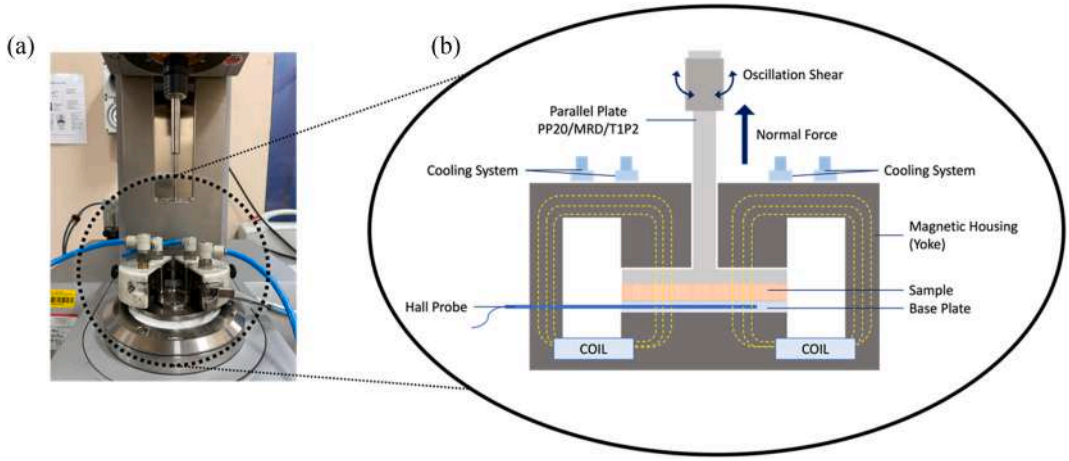

Fig. 2. Experimental set-up of rheological analysis where; (a) close-up image and (b)schematic illustration of MCR302.

carried out using variable pressure scanning electron microscopy (VP-SEM) (JEOL JSM-IT300LV), to observe the distribution of CIPs embedded into the porous structure of the fabricated samples. For VP-SEM, the samples of 1 mm thickness were prepared and coated with a thin layer of platinum before analysis. This step prevented any possible surface charging, providing a homogeneous surface for analysis and imaging. The cross-section of the samples was examined at an acceleration voltage of 10 kV under magnifications of x500.

3. Results and discussion

3.1. Density and porosity analysis

Based on the results as tabulated in Table 2, PU foam exhibited the density, ρ of 0.20 g/ml. Since the chemical reactant used to produce the PU foam is about 1.03 g/ml and 1.00 g/ml for polyol and isocyanate respectively, the calculated $\rho_{relative}$ of the PU foam is 0.20. Then, the ρ of MR foams increased accordingly as the CIPs was added to the PU matrix. This indicates that the presence of CIPs has a significantly influence the total mass of the overall material's compositions as compared to PU foam, and the finding was supported by previous studies [18,22,26,27,33,34]. In fact, the increasing trend of the ρ was observed when constrained volume foaming process was applied during the fabrication of MR foams, as stated in Table 1. As the volume of closed mold was reduced, the ρ of MR foams has been increased. The highest ρ among the MR foam samples was possessed by sample D with 0.90 g/ml, followed by samples C, B and A with the ρ of 0.59, 0.45 and 0.43 g/ml, respectively. As the density is related to the ratio of mass to volume of a sample, the decreasing volume of a closed mold has subsequently increased the material concentrations within the constrained volumes. Then, the distribution of CIPs would become more compact which resulted in the increment of the respective ρ. Indeed, the $\rho_{relative}$ of sample A, B, C and D are around 0.10, 0.11, 0.15 and 0.23, respectively indicating the denser MR foam with limited volumes. The data also has been interpreted in the graph as shown in Fig. 3.

On the other hand, formation of voids within the MR foam's structure has primarily related to the porosity, φ and it is another parameter that also influence the resultant properties of porous materials. Presence of φ in the structure of MR foam may impede the magnetic flux that flow through the samples during the on-state condition which ultimately disrupted the rheological properties of MR foam [25]. Thus, larger φ would weaken more the resultant stiffness of the material. As shown in Table 2, the φ of PU foam was noted about 79.79 % however, the φ increased by about 9 % when the CIPs of 75 wt% was added to the PU matrix, particularly with free foaming process (Sample A). This finding somehow agrees with the previous studies that incorporating particles to the polymer matrix has increased the φ of the composite materials [35–37]. It might be due to the incorporated CIPs has facilitated the nucleation of pores during foaming process of the MR foam. Nevertheless, albeit the foaming process of sample A and B was different, with B experienced constraint volume foaming process of 100 %, the percentage of φ value was almost similar, with B reduced by about 0.5 %. It is attributed to the similar expansion volume of MR foams during the foaming process. Meanwhile, sample C and D show further decreasing trend of the φ when each MR foam underwent constraint volume foaming conditions of 75 % and 50 %, respectively. In such conditions,

Table 2
Details on the density and porosity of the fabricated MR foam samples.

Sample	Density, ρ (g/ml)	Relative Density, $\rho_{relative}$	Porosity, φ (%)
A	0.43	0.10	89.06
B	0.45	0.11	88.62
C	0.59	0.15	84.98
D	0.90	0.23	77.24

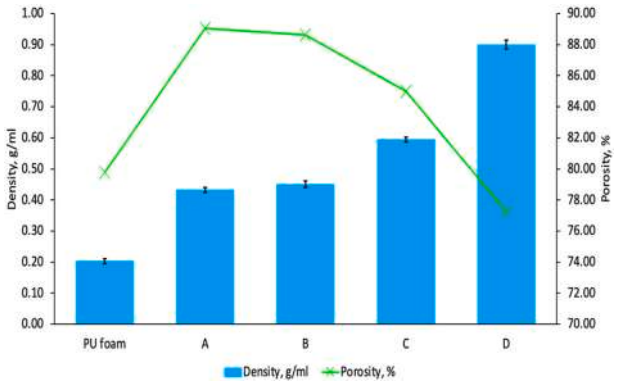

Fig. 3. Trend of density and porosity of foam samples fabricated via different constrained volume foaming process.

MR foam have more limited spaces for the formation and growth of pores, resulted in a denser and packed structure of MR foam, and simultaneously decreased the fraction of void [22]. In fact, sample C exhibited the φ of about 84.98 % while sample D has around 77.24 %. Besides, the constraint volume foaming process might also reduce the deformation of pores which predominantly caused by the coalescence of pore structures [38]. Therefore, it can be seen that the constraint volume foaming approach has a significant effect on the alteration of MR foam structure that also caused the φ reduction of the material. The corresponding morphological analysis of MR foams will be provided later in this study.

3.2. Strain dependent analysis

In this study, a strain sweep test was conducted to observe the effect of constrained foaming in improving the G' of MR foams. The changes in the initial value of G' fabricated with different mold lengths was observed. The test was carried out with a regulated range of shear strains from 0.001 to 10 % at a constant frequency of 1 Hz under oscillatory shear mode. In addition, the change and limit of LVE of MR foam was determined to ensure further testing, which includes current sweep and frequency sweep, were done within its elastic region. The LVE region provides information about the material rigidity by providing the range in which the material can withstand the given shear strains without deteriorating the structure. For the sake of comparison, Fig. 4 includes the LVE region and G' of the PU foam without the CIPs addition. Compared to MR foams, PU foam exhibits the extensive LVE region for both off-state (Fig. 4 (a)) and on-state (Fig. 4 (b)) conditions. In terms of the G', PU foam possess about 52 kPa, the lowest value of G' and it remains constant for the shear strain up to 10 %, indicating its pronounced viscoelastic characteristics as compared to composite foams. In fact, the trend is similar for both conditions showing its nature behavior of not responding to the magnetic field stimuli. Then, it can be observed that the presence of CIPs has increased the G' of the MR foams, resulting the stiffer materials but it compromised with the shorter LVE region, than the PU foam.

The LVE region of MR foam samples was determined according to the previous recommended work with the LVE limit point set at a 10 % deviation from the approximated straight line of the G' [39,40]. As in Fig. 4 (a), the sample A which was fabricated via free-foaming process exhibited the second longest LVE region among the MR foam samples, particularly in the range of 0.01 %–4 % of the shear strain. However, when constraint foaming was introduced to the fabrication process, the LVE region was slightly shorter, as shown by sample B. The volume of constraint foaming was further reduced by 25 % (sample C) and 50 % (sample D). As a result, the LVE regions were reduced by approximately 2 % and 1.5 % of shear strain, respectively. A similar decreasing trend is observed at the on-state condition, as shown in Fig. 4 (b). In this LVE

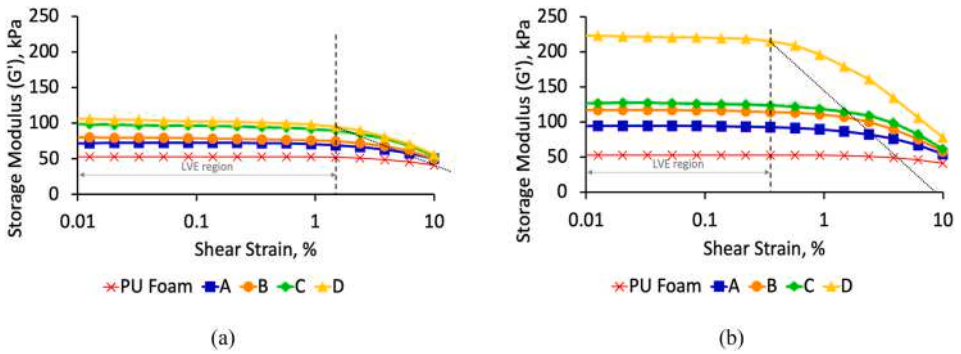

Fig. 4. LVE region and storage modulus of MR foam at (a) off-state and (b) on-state test conditions.

determination, the maximum applied current of 4 A was chosen because the region representing MR foam elasticity was the shortest at the highest magnetic field strength. Previous research [21] reported the same LVE region trend and stated that a higher content of magnetic particles led to a shorter LVE region. In other words, shorter LVE regions indicated that the samples stiffened when applying the magnetic field. Thus, the LVE region for sample D was further reduced from 1.5 % to 0.5 % of shear strain when compared with the off-state condition. For these reasons, it was deduced that the compact distribution of CIPs causes the samples to be stiffer. The decreasing trend in the LVE region was due to a network formed by the matrix-filler interaction [21,41].

On the other hand, a compact distribution of magnetic particles denoted that it could enhance the capability of MR foam in terms of G' in the LVE region. As shown in Fig. 4, the initial G' value was higher when the constraint volume foaming process was applied to the MR foam fabrication. Furthermore, the initial G' value increased when the constraint foaming volume was reduced. At off-state conditions, the initial G' of sample A was 70 kPa, which was comparable to a previous study that focused on a free-foaming approach [3,42]. The values were higher for sample B (80 kPa) and continued to increase for samples C (100 kPa) and D (105 kPa), indicating that CIP distribution was more compact than the free foaming process.

It was noted that constraint volume foaming has a great influence on the initial G' of MR foam, particularly at off-state conditions, where the behavior mainly depended on the matrix modulus. This phenomenon is a common MR foam behavior; as the amount of magnetic particles increases, so does the initial G' [21,41]. Meanwhile, at on-state conditions, all samples showed an increment in the initial G' compared to their off-state condition. Based on [3], the G' of free foaming MR foam has only a slight increase of around 1–5 kPa under the magnetically induced current between 0 and 4 A. Conversely, MR foam fabricated using the constraint volume foaming process has a significant increment. In particular, the values ranged from 27 to 39 kPa. Eventually, the compact CIP distribution in constrained foaming MR foams increased the G' value. This finding agrees with a previous research that the increasing G' trend was due to higher concentration of particles per unit volume of the samples [34,43]. Consequently, this would contribute positively towards potential applications.

Additionally, a better understanding of the effect of the constraint

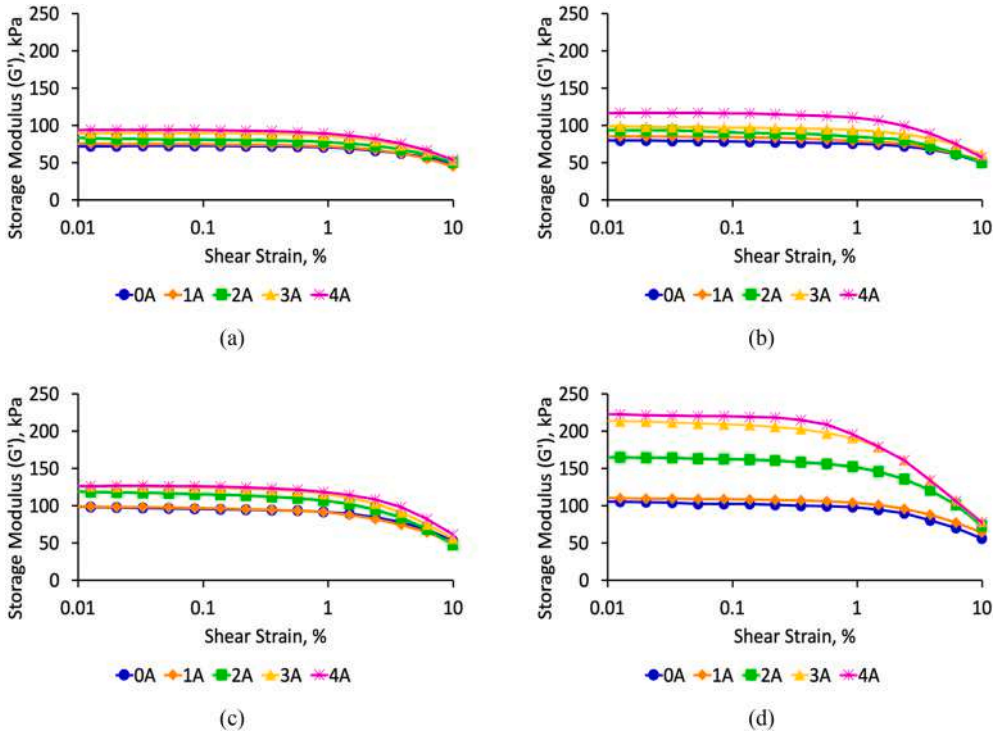

Fig. 5. Strain sweep for MR foam fabricated via (a) free foaming and different constraint volumes foaming, indicated by (b) 100%, (c) 75% and (d) 50% of mold length.

volume foaming process on MR foam can be observed in Fig. 5. The initial G' for all samples rose with the increasing applied current throughout Fig. 5 (a)–(d). The magnetic particles were rapidly magnetized in the presence of a magnetic field and aligned according to the magnetic field direction due to the magnetic interaction, which contributed to the increment of G' [44–46]. In another observation, the G' of sample B was higher than sample A when compared to the 100 % of mold volume even though they have the same expansion ratio of MR foam. This is caused by a higher amount of gas trapped during nucleation due to the constrained foaming process of MR foam, resulting in enhanced pore development in the foam structure [6]. For this reason, higher G' was observed in sample B than in sample A, mainly due to compact CIP distribution during the constrained foaming process.

Apparently, as portrayed in Fig. 5(b)–(d), the initial G' gradually increased with decreasing mold length when a constraint volume foaming process was introduced. The difference in the initial G' at applied current of 1–4 A for sample B was not distinct, but as the mold volume mold was reduced (samples C and D), a higher increment of the initial G' was observed. Almost the same differences and pattern were also observed for all values of the remaining G'. The CIPs distribution became more compact, reducing the gaps between the particles in the matrix struts of foam. Therefore, more chain-like structures were formed, resulting in a higher G'. This explains the apparent difference in G' between the minimum (1 A) and maximum applied current (4 A) at the lowest volume constraint of 50 % (Fig. 5(d)). The LVE region at these points decreased distinctly, indicating that the G' of MR foam has reached its saturation point, limiting the formation of molecular chain within the MR foam. As a result, the matrix could not retain the G' resulting in a temporary structure deformation, contributing to a shorter LVE region. Undoubtedly, constraint volume foaming process has significantly affected the G' of MR foam.

3.3. Magnetic field dependent analysis

The magnetic field-dependent test of the fabricated MR foams was conducted under constant strain and frequency of 0.1 % and 1 Hz, respectively. Fig. 6 portrays the effect of the constraint volume foaming process on the G' of MR foam under different magnetic field values.

The absolute MR effect was extracted from this analysis to provide more details on the effect of different foaming processes on the rheological properties of MR foam and displayed in Table 3. The magneto-rheological effect is one of the key parameters used to measure the responsiveness of MR materials in terms of the changeable G' under the influence of applied magnetic fields [2,47], where it was described as an absolute MR effect in this study. The output would be advantageous as the materials could gain higher potential for application in controllable

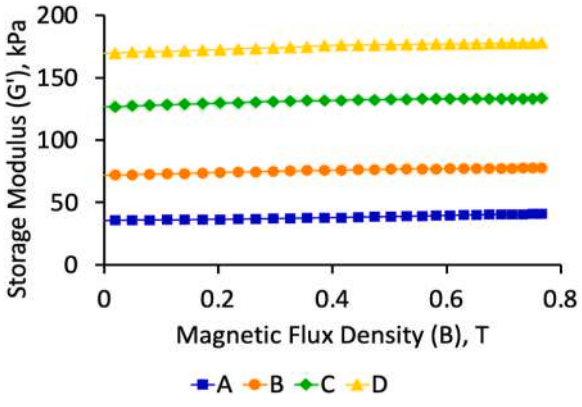

Fig. 6. The graph of storage modulus of MR foam against magnetic flux density.

Table 3
The absolute MR effect of fabricated MR foams.

Sample	Initial Storage Modulus (G'_0), kPa	Maximum Storage Modulus (G'_{max}), kPa	Absolute MR Effect (ΔG), kPa
A	35.7	40.9	5.2
B	71.8	77.6	5.8
C	126.7	133.3	6.6
D	169.6	178.0	8.4

semi–active actuators, smart soft grippers, and innovative sensor devices. Thus, the absolute MR effect (ΔG) can be evaluated from the difference between the maximum storage modulus (G'_{max}) and initial storage modulus (G'_0) with the influence of magnetic field, as presented in Equation (4).

$$\Delta G = G'_{max} - G'_0 \tag{4}$$

Based on the results displayed in Fig. 6, the G' of all samples shows an increasing trend in proportion to an increase in magnetic flux density, ranging from 0 to 0.774 T. Particularly, the G'_0 of MR foam fabricated using the free-foaming process (sample A) was about 35.7 kPa. When the constraint volume foaming process was introduced to MR foam, G'_0 increased to 71.8, 126.7 and 169.6 kPa, as indicated by samples B, C and D, respectively. The increment was believed to be a consequence of the compact distribution effect of CIPs in the struts of MR foam. The MR effect of free-foaming MR foam was 5.2 kPa, which agrees with previous studies [3,22,42]. It can be seen that the MR effect of sample B slightly increased by 0.6 kPa, particularly from 5.2 to 5.8 kPa. In fact, with further reduction of MR foam constraint volume, the MR value increased to 6.6 and 8.4 kPa for samples C and D, respectively.

The inclined trend of the MR effect in this study corresponds to similar conclusions of previous studies [21,33], where the increase of the MR effect was significantly due to the increment of the magnetic particle content in MR foam. Further, it was reported that the MR effect could be adjusted by adjusting the content of magnetic particles and magnetic field strength [33]. Likewise, more chain-like structures were formed because of the tendency of CIPs to align accordingly to the higher magnetic field. Consequently, a smaller difference in the increment of modulus for sample A was because of the difficulty in the stress transfer due to weak interaction between the particles, thereby contributing to a smaller MR effect of MR foam. On the other hand, the presence of constraint volume foaming process of MR foam has successfully enhanced the MR effect, as demonstrated by samples B, C, and D. The weak interaction between CIPs under the influence of magnetic field was improved via compact distribution of CIPs, which reduced the gaps between particles. As a result, CIPs became more sensitive to the change in the magnetic field, resulting in effective stress transfer within MR foam. Thus, more significant MR effect of MR foam could be observed. Even though each MR foam showed small increase in MR effect, the rising G' value nevertheless indicated the MR foam had undergone a structural change. A larger influence of the magnetic field resulted in more magnetic interactions between the CIPs, increasing G'.

3.4. Morphological characterization

Fig. 7 depicts the microstructure of the fabricated MR foams under observation using an optical microscope. In general, the pore structure is an essential parameter in determining porous materials' properties [16,17]. In other words, the morphological parameters, such as pore size, would influence the final properties of MR foam.

Fig. 7 (a) shows that sample A has the largest size of pores than the other samples. Meanwhile Fig. 7 (b)–(d) demonstrate that the pore sizes decreased as the volume of constraint foaming process reduced, with sample D exhibited the smallest average pore sizes and possess better homogenous of pores distribution. The role of CIPs as a nucleating agent

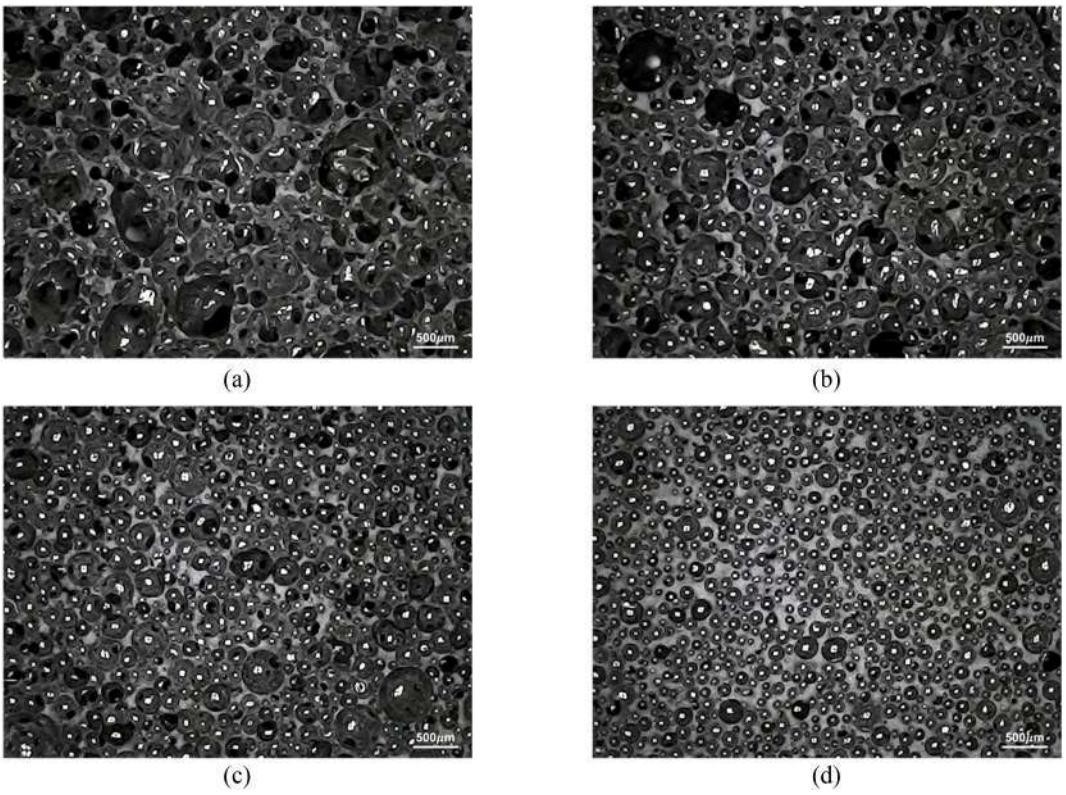

Fig. 7. The micrographs of MR foam fabricated via (a) free foaming (sample A) and constraint volume foaming of (b) 100% (sample B), (c) 75% (sample C) and (d) 50% (sample D) mold lengths.

has promoted more formation of pores under constraint volume condition [18]. Therefore, Fig. 8 shows the information on the number of estimated nucleated pores for all MR foam samples which was calculated by the ratio between the average number of pores per unit area (1 mm^2) and its $\rho_{relative}$. Sample A and B have the average pores of approximately 5 and 6 pores per unit area, respectively. This indirectly correspond to the porosity finding as the sample A and B has a similar porosity value. As the volume of constrained foaming was reduced, the average numbers of nucleated pores increased to about 10 and 16 pores for samples C and D, respectively. Indeed, sample D has the highest relative density of 0.23, indicating that the sample contained more CIPs per unit area. Similar observation was made in the previous study that a higher density of foam resulted in a smaller size of pores [43]. In fact, larger amount of CIPs, particularly with 75 wt% has significantly affected the growth process of pores and led to the change in the morphological structure of MR foams [21,33]. Based on observation, the estimated nucleated pores showed an increasing trend where sample A, B, C and D has estimation of 46, 53, 67 and 70 nucleated pores accordingly. In addition, there were studies which reported that the morphological structure of MR foams could be regulated by manipulating the alignment of particles using time-dependent magnetic fields during the fabrication process [34,43]. However, the resulting MR foam would be known as an anisotropic MR foam instead of isotropic-type and manipulating the arrangement of CIPs in the PU foam is another approach to enhance the storage modulus of MR foam.

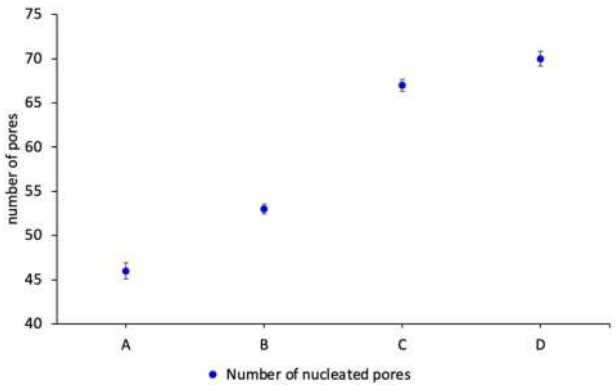

Fig. 8. The estimated number of nucleated pores of the fabricated samples.

For this reason, densely packed CIPs that distributed in the constraint volume of MR foam played a significant role in controlling the pores dimension, causing in smaller pores formed in the foam structure. Consequently, convenient size and more homogeneous distribution of pores could be seen, especially in sample D, compared to the other samples due more compact CIPs distributions. The structure refinement also correlated to the porosity reduction of the samples. Constrained foaming process via reduced mold volume during the fabrication have minimized the formation of coalesced structures in MR foams. Fig. 9 shows the magnified region of the morphological image of MR foams, focusing on the strut area that were observed by the VP-SEM. All MR foams including the free foaming process (a) and the constraint foaming of 100 % (b), 75 % (c) and 50 % (d) consists of similar strut structures. All look grumbling since the embedded CIPs were distributed in that area, attributed to the in-situ foaming process of the MR foams. The observed protruding granulates are CIPs and the background base material is the PU matrix. Overall, the CIPs showed a uniform dispersion entire the matrix strut areas, enclosed with the pores and this resultant microstructure has influenced the properties alteration of MR foams, especially in terms of the G' and its MR effect.

The CIP concentration might impact the MR foam properties, especially the ability to provide higher G' [21]. A mechanism based on the effect of constraint volume foaming process of MR foam towards its rheological properties is proposed as a result of understanding the microstructure characteristics obtained from the morphological

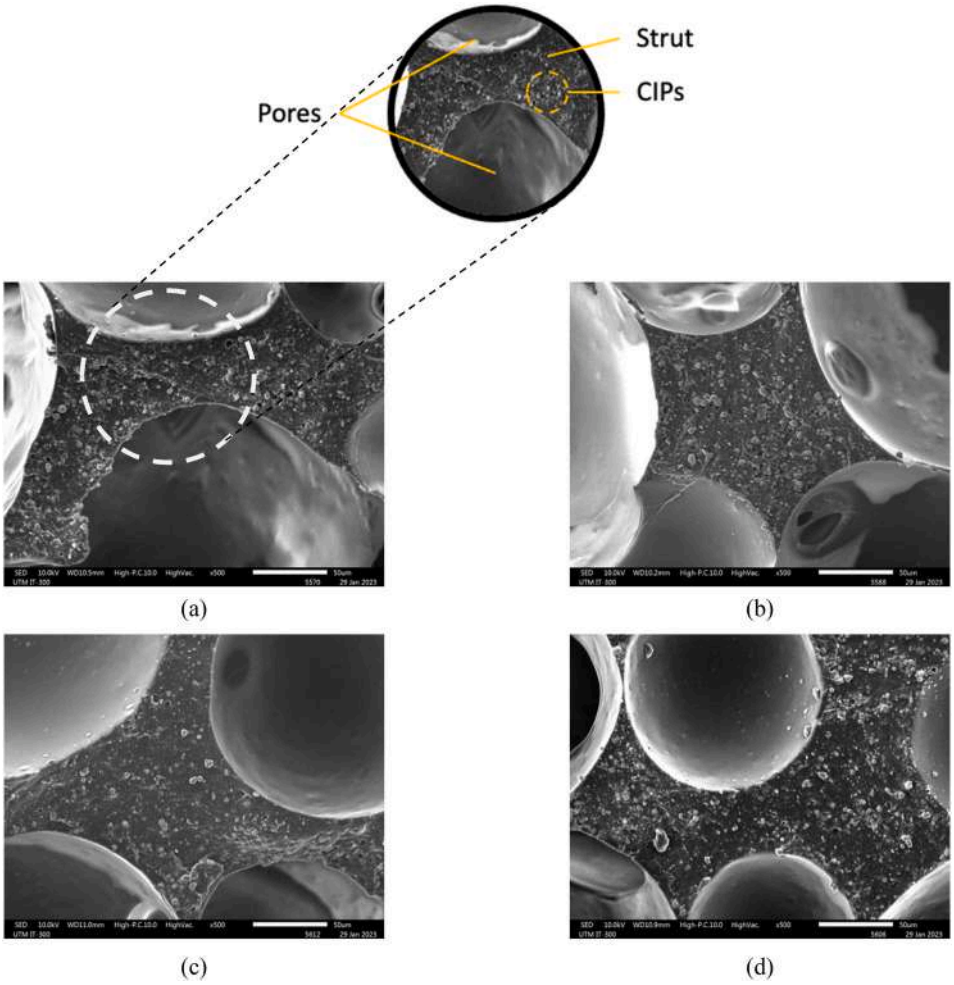

Fig. 9. Cross-section image of MR foam samples fabricated via (a) free foaming (sample A) and constraint volume foaming of (b) 100 % (sample B), (c) 75 % (sample C) and (d) 50 % (sample D) observed by using VP-SEM under magnification of x500.

analysis.

Fig. 10 depicts the mechanism of MR foams, illustrating the CIPs distribution over the strut area, and demonstrates the behavior of MR foams at with and without the external magnetic field. Referring to the rheological properties as discussed previously, sample B exhibited higher $G_0^{'}$ than the sample A even though both samples have similar expansion volume of foaming process. It is due to slightly higher amount of gas trapped in the structure during constraint foaming of B, triggering the improvement of pore structure of MR foam [6]. Additionally, as the volume of constraint foaming was reduced, a greater $G^{'}$ of MR foam was obtained, indicating that the gaps between the CIPs were reduced/minimized. The formation of pores also has been improved as homogeneity of pores size have been observed accordingly. Thus, a more compact area that consists of smaller pores and CIPs distributed were noted, as illustrated in Fig. 10 (a) (i-iv). An analogy from the Hall-Petch equation related to the strengthening of material by grain size reduction can be adapted in this analysis. It stated that the increment in yield stress of a material is compromised with the reduction of the grains diameter of the material [48]. Indeed, smaller pores size of MR foam has contributed to the increasing $G^{'}$ of the MR foam. Thus, the refinement of pores provided an important factor to improve the rheological properties of the MR foams. In fact, at the off-state condition, the behavior of MR foams is mainly dependent on the composite foam itself and the formation of uniform structure has a strong correlation towards the resultant behavior of the material.

On the other hand, further increased in $G^{'}$ was noted when the magnetic field was applied to the MR foams, showing that there were interactions between the CIPs as the magnetic particles were attempted to align according to the flow and direction of magnetic field. Since the MR foams become more compact with reducing gap between the particles, the interparticle interactions towards the magnetic field has been enhanced, as illustrated in Fig. 10 (b) (i-iv). As a result, the MR foams become more stiffer.

4. Conclusion

This study proposed an alternative approach for the fabrication process of MR foam. Flexible MR foams with fixed 75 wt% of CIPs were successfully fabricated using two foaming approaches, namely free foaming and constraint volume foaming processes. Subsequently, the volume of constraint foaming MR foam was further reduced by 25 % and 50 % to observe the effect of constraint foaming towards enhancing rheological properties, particularly in terms of storage modulus, MR effect, and the morphological structure of MR foam. It was observed that under the influence of applied strains, 100 % volume of constraint foaming MR foam enhanced the storage modulus compared to free foaming MR foam despite possessing the same expansion ratio. When the volume was further reduced by 25 % and 50 %, the storage modulus continued to increase in both analysis conditions, i.e., off- and on-state conditions.

Similarly, under the influence of a magnetic field, the absolute MR effect was enhanced to 8.4 kPa at 50 % volume of constraint forming in contrast to 5.2 kPa at free foaming MR foam. These enhancements were

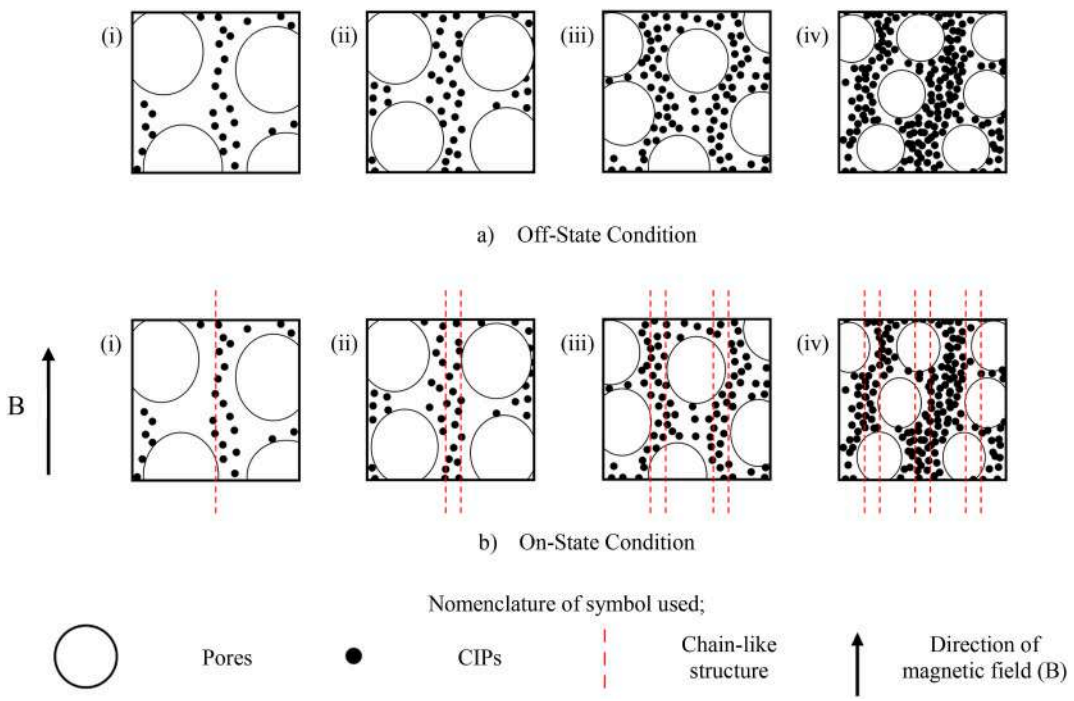

Fig. 10. The illustration of behavior of (i) free foaming, constrained foaming (ii) 100%, (iii) 75% and (iv) 50% volumes of MR foam samples at (a) off- and (b) on-state conditions.

attributed to the compact CIP distribution, which can be supported by increasing the relative density of each sample. Another reason is that the constraint volume of the foaming process has reduced the MR foam porosity, significantly affecting the rheological properties, which was portrayed in the enhancement of rheological analysis in this study. Hence, introducing constraint foaming in the fabrication of MR foam positively impacted the porous structure's rheological properties and structural properties.

Author statement

We sincerely appreciate the opportunity to further improve the manuscript. We have diligently make the necessary corrections according to reviewer's comments. For the ease of identification, corrections has been highlighted in ORANGE colour. With all these corrections and improvements, we respectfully submit this revised version of the manuscript to your esteemed journal for your thoughtful review. We are really hoping that the manuscript aligns with the standard of excellence set by the Polymer Testing and will be acceptable for publication.

Declaration of competing interest

The authors declare that they have no known competing financial interests or personal relationships that could have appeared to influence the work reported in this paper.

Data availability

Data will be made available on request.

Acknowledgments

The authors would like to acknowledge the financial support from the Ministry of Education Malaysia under Fundamental Research Grant Scheme (FRGS) (FRGS/1/2022/TK10/UTM/02/75) and Japan International Cooperation Agency Fund (JICA Fund) R. K130000.7343.4B696. M. S. wishes to thank the Czech Science Foundation [23-07244S] for the financial support.

References

[1] V. Volpe, M. D'Auria, L. Sorrentino, D. Davino, R. Pantani, Magneto-mechanical behavior of elastomeric carbonyl iron particles composite foams produced by foam injection molding, J. Magn. Magn Mater. 466 (2018) 44–54.
[2] N.S. Muhazeli, N.A. Nordin, U. Ubaidillah, S.A. Mazlan, S.A. Abdul Aziz, N. Nazmi, I. Yahya, Magnetic and tunable sound absorption properties of an in-situ prepared magnetorheological foam, Materials 13 (2020) 5637–5652.
[3] R. Norhaniza, S.A. Mazlan, U. Ubaidillah, M. Sedlacik, S.A.A. Aziz, N. Nazmi, K. Homma, S. Rambat, Sensitivities of rheological properties of magnetoactive foam for soft sensor technology, Sensors 21 (2021) 1660–1678.
[4] L. Sorrentino, M. Aurilia, G. Forte, S. Iannace, Anisotropic mechanical behavior of magnetically oriented iron particle reinforced foams, J. Appl. Polym. Sci. 119 (2011) 1239–1247.
[5] K. Nadella, V. Kumar, W. Li, Constrained solid-state foaming of microcellular panels, Cell. Polym. 24 (2005) 71–90.
[6] H. Guanghong, W. Yue, Microcellular foam injection molding process, in: Some Crit. Issues Inject. Molding, InTech, 2012, pp. 175–202.
[7] L. Wang, W. Cui, H.-Y. Mi, D. Hu, M.F. Antwi-Afari, C. Liu, C. Shen, Fabrication of skinless cellular poly (vinylidene fluoride) films by surface-constrained supercritical CO2 foaming using elastic gas barrier layers, J. Supercrit. Fluids 184 (2022) 105562–105571.
[8] I. Duarte, M. Vesenjak, L. Krstulović-Opara, Compressive behaviour of unconstrained and constrained integral-skin closed-cell aluminium foam, Compos. Struct. 154 (2016) 231–238.
[9] S. Tan, T. Abraham, D. Ference, C.W. Macosko, Rigid polyurethane foams from a soybean oil-based Polyol, Polymer (Guildf) 52 (2011) 2840–2846.
[10] A.N.J. Spörrer, V. Altstädt, Controlling morphology of injection molded structural foams by mold design and processing parameters, J. Cell. Plast. 43 (2007) 313–330.
[11] J. Chen, L. Yang, D. Chen, Q. Mai, M. Wang, L. Wu, P. Kong, Cell structure and mechanical properties of microcellular PLA foams prepared via autoclave constrained foaming, Cell, Polym 40 (2021) 101–118.
[12] S. Siripurapu, J.M. DeSimone, S.A. Khan, R.J. Spontak, Low-temperature, surface-mediated foaming of polymer films, Adv. Mater. 16 (2004) 989–994.
[13] J. Jiang, H. Zheng, H. Liu, W. Zhai, Tunable cell structure and mechanism in porous thermoplastic polyurethane micro-film fabricated by a diffusion-restricted physical foaming process, J. Supercrit. Fluids 171 (2021) 105205–105214.
[14] A.R. Kennedy, Effect of foaming configuration on expansion, J. Mater. Sci. 39 (2004) 1143–1145.
[15] M. Li, X. Cao, Y. Luo, Cell structure and impact properties of foamed polystyrene in constrained conditions using supercritical carbon dioxide, Iran, Polym. J. 23 (2014) 775–781.
[16] J. Li, X. Liao, Q. Jiang, W. Wang, G. Li, Creating orientated cellular structure in thermoplastic polyurethane through strong interfacial shear interaction and

supercritical carbon dioxide foaming for largely improving the foam compression performance, J. Supercrit. Fluids 153 (2019) 104577–104591.
[17] G. Wang, G. Wan, J. Chai, B. Li, G. Zhao, Y. Mu, C.B. Park, Structure-tunable thermoplastic polyurethane foams fabricated by supercritical carbon dioxide foaming and their compressive mechanical properties, J. Supercrit. Fluids 149 (2019) 127–137.
[18] M. Nar, C. Webber, N. Anne D'Souza, Rigid polyurethane and kenaf core composite foams, Polym. Eng. Sci. 55 (2015) 132–144.
[19] S. Siripurapu, J.M. DeSimone, S.A. Khan, R.J. Spontak, Controlled foaming of polymer films through restricted surface diffusion and the addition of nanosilica particles or CO 2 -philic surfactants, Macromolecules 38 (2005) 2271–2280.
[20] N.S. Muhazeli, N.A. Nordin, S.A. Mazlan, S.A. Abdul Aziz, Ubaidillah, N. Nazmi, Mini review: an insight on the fabrication methods of smart magnetic polymer foam, J. Magn. Magn Mater. 534 (2021) 168038–168048.
[21] N.S. Muhazeli, N.A. Nordin, S.A. Mazlan, N. Rizuan, S.A. Abdul Aziz, A.Y. Abd Fatah, Z. Ibrahim, U. Ubaidillah, S.-B. Choi, Characterization of morphological and rheological properties of rigid magnetorheological foams via in situ fabrication method, J. Mater. Sci. 54 (2019) 13821–13833.
[22] R. Norhaniza, S.A. Mazlan, Ubaidillah, S.A. Abdul Aziz, N. Nazmi, N.A. Yunus, Enhancement of sensitivity of magnetostrictive foam in low magnetic fields for sensor applications, Polymer (Guildf) 211 (2020) 123083–123092.
[23] S. Zaidi, M. Maselli, C. Laschi, M. Cianchetti, Actuation technologies for soft robot grippers and manipulators: a review, Curr. Robot. Reports. 2 (2021) 355–369.
[24] M.A. Tasin, S.A.A. Aziz, S.A. Mazlan, M.A.F. Johari, N.A. Nordin, S.Y.M. Yusuf, S.-B. Choi, I. Bahiuddin, Magnetostriction enhancement in midrange modulus magnetorheological elastomers for sensor applications, Micromachines 14 (2023) 767–782.
[25] R. Norhaniza, S.A. Mazlan, S.A. Abdul Aziz, Ubaidillah, N.A. Nordin, N. S. Muhazeli, Relationship between the response of microscopic and magnetic properties with highly uniform dispersion of carbonyl iron particles in magnetorheological polyurethane foam, Smart Mater. Struct. 29 (2020) 115012–115021.
[26] M. D'Auria, D. Davino, R. Pantani, L. Sorrentino, Polymeric foam-ferromagnet composites as smart lightweight materials, Smart Mater. Struct. 25 (2016), 055014–055027.
[27] S.N. Ishak, P.L. Teh, U.L. Du Ngoc, C.K. Yeoh, Porous epoxy: effect of mixing sequences (ELH versus EHL) using toluene as extraction medium via ultrasonic technique, Int. J. Polym. Sci. 2016 (2016) 1–5.
[28] Raja Yateesh Yadav, Dr E.S. Prakash, Experimental determination of relative density and percentage porosity of open cell aluminium foam produced from sand salt mould method, Int. J. Eng. Res. V5 (2016) 152–154.
[29] Z. Hussain, N.S.A. Suffin, Microstructure and mechanical behaviour of aluminium foam produced by sintering dissolution process using NaCl space holder, J. Eng. Sci. 7 (2011) 37–49.
[30] T.H.M. Lau, L.L.C. Wong, K.-Y. Lee, A. Bismarck, Tailored for simplicity: creating high porosity, high performance bio-based macroporous polymers from foam templates, Green Chem. 16 (2014) 1931–1940.
[31] E. Malewska, S. Bąk, A. Prociak, Effect of different concentration of rapeseed-oil-based polyol and water on structure and mechanical properties of flexible polyurethane foams, J. Appl. Polym. Sci. 132 (2015) 42372–42383.
[32] P. Cimavilla-Román, M. Santiago-Calvo, M.Á. Rodríguez-Pérez, Dynamic Mechanical Analysis during polyurethane foaming: relationship between modulus build-up and reaction kinetics, Polym. Test. 103 (2021), 107336.
[33] Q. Gong, J. Wu, X. Gong, Y. Fan, H. Xia, Smart polyurethane foam with magnetic field controlled modulus and anisotropic compression property, RSC Adv. 3 (2013) 3241–3248.
[34] D. Davino, M. D'Auria, R. Pantani, L. Sorrentino, Reinforced smart foams produced with time-profiled magnetic fields, Polymers 13 (2020) 24–42.
[35] M. Schümann, N. Seelig, S. Odenbach, The effect of external magnetic fields on the pore structure of polyurethane foams loaded with magnetic microparticles, Smart Mater. Struct. 24 (2015), 105028.
[36] M. Schümann, S. Günther, S. Odenbach, The effect of magnetic particles on pore size distribution in soft polyurethane foams, Smart Mater. Struct. 23 (2014), 075011–075021.
[37] S. S, P. S, A. A, S. M, U. M, H. T, L. E, P.-R. Y, T. A, Porous hydroxyapatite-magnetite composites as carriers for guided bone regeneration, Front. Nanosci. Nanotechnol. 3 (2017) 1–9.
[38] M.-C.D. Jawhar, D. Blanc, P. Chaumont, P. Cassagnau, Study of the coalescence mechanisms during silicone foaming, Macromol. Mater. Eng. 299 (2014) 336–343.
[39] I. Agirre-Olabide, J. Berasategui, M.J. Elejabarrieta, M.M. Bou-Ali, Characterization of the linear viscoelastic region of magnetorheological elastomers, J. Intell. Mater. Syst. Struct. 25 (2014) 2074–2081.
[40] I. Agirre-Olabide, M.J. Elejabarrieta, M.M. Bou-Ali, Matrix dependence of the linear viscoelastic region in magnetorheological elastomers, J. Intell. Mater. Syst. Struct. 26 (2015) 1880–1886.
[41] J. Fröhlich, W. Niedermeier, H.-D. Luginsland, The effect of filler–filler and filler–elastomer interaction on rubber reinforcement, Composer Part A Appl. Sci. Manuf. 36 (2005) 449–460.
[42] R.E.M. Khaidir, N.A. Nordin, S.A. Mazlan, H. Abd Rahman, Ubaidillah, S.A. Abdul Aziz, N. Nazmi, Stiffness enhancement of magnetorheological foam by structural modification using silica nanoparticles additive, Front. Mater. 9 (2022) 1–14.
[43] M. D'Auria, D. Davino, R. Pantani, L. Sorrentino, Magnetic field-structuring as versatile approach to shape the anisotropic mechanical response of composite foams, Composites, Part B 212 (2021) 108659–108672.
[44] R.Z.A. Rashid, N.A. Yunus, S.A. Mazlan, N. Johari, S.A.A. Aziz, N.A. Nordin, M.H. A. Khairi, M.A.F. Johari, Temperature dependent on mechanical and rheological properties of EPDM-based magnetorheological elastomers using silica nanoparticles, Materials 15 (2022) 2556–2571.
[45] Y. Wan, Y. Xiong, S. Zhang, Temperature dependent dynamic mechanical properties of Magnetorheological elastomers: experiment and modeling, Compos. Struct. 202 (2018) 768–773.
[46] Q. Wen, L. Shen, J. Li, S. Xuan, Z. Li, X. Fan, B. Li, X. Gong, Temperature dependent magneto-mechanical properties of magnetorheological elastomers, J. Magn. Magn Mater. 497 (2020) 165998–166004.
[47] R.Z. Abd Rashid, N. Johari, S.A. Mazlan, S.A. Abdul Aziz, N.A. Nordin, N. Nazmi, S. N. Aqida, M.A.F. Johari, Effects of silica on mechanical and rheological properties of EPDM-based magnetorheological elastomers, Smart Mater. Struct. 30 (2021) 105033–105046.
[48] Z.C. Cordero, B.E. Knight, C.A. Schuh, Six decades of the Hall–Petch effect – a survey of grain-size strengthening studies on pure metals, Int. Mater. Rev. 61 (2016) 495–512.